

Melting and melt structure of MgO at high pressures

Ronald E. Cohen and Z. Gong

Center for High Pressure Research, Geophysical Laboratory, 5251 Broad Branch Road N.W., Washington, D.C. 20015-1305

(Received 22 February 1994; revised manuscript received 14 April 1994)

By performing large-scale molecular-dynamics simulations of clusters of MgO we investigate the fundamental physics of melting, and the effects of pressure on melt and crystal structure along the melting curve from zero pressure to 300 GPa. We find that melting occurs at constant root-mean-squared (rms) displacements relative to the average near-neighbor distance over the entire pressure range, in agreement with Lindemann's predictions of 1910, and contrary to previous studies that indicate failure of Lindemann's law for nonmonatomic substances. The high-pressure validity of Lindemann's law supports one-phase models for melting. The liquid structure varies along the melting curve, becoming more crystal-like with increasing pressure with average coordinate number changing from 4.5 to 6, and $\Delta V/V_c$ tends to zero with increasing pressure. Trends in thermodynamic functions and structure indicate that in the extreme pressure limit, melting is characterized only by dynamical changes such as onset of rapid diffusion, and not by local structural changes, since high pressure favors efficient packing of the liquid as well as the solid.

I. INTRODUCTION

The physics of melting, particularly the relationship between melting and intrinsic instabilities of crystals and liquids, has remained a subject of great interest for most of the century beginning at least as early as Lindemann's 1910 paper¹ relating melting to a threshold for atom displacements from their equilibrium positions. Melting has since been related to instabilities in the crystal as temperature increases,²⁻⁵ to an instability in the liquid with increasing order as temperature decreases,⁶ and to an instability in the crystal related to the growth of defects such as dislocations.⁷ In this study we have used a first-principles approach, and have applied the same nonempirical, many-body potential, the potential-induced breathing or PIB model,⁸ for MgO using both molecular dynamics and lattice dynamics to understand the melting process and how it relates to lattice instabilities. We have chosen to study MgO since it is not complicated by solid-state phase changes up to 500 GPa,^{9,10} and because an accurate, well-tested potential is available.⁹ MgO is also an end member of magnesiowustite (Mg,Fe)O, which is believed to be a major phase in the Earth's lower mantle, and represents a simple analogue for melting of close-packed oxides and silicates, an understanding of which is of great importance to geophysics. By using the massively parallel CM-2 and CM-5 supercomputers we were able to run for long times to reduce hysteresis and to obtain accurate values for static and dynamical correlation functions such as rms displacements.

Molecular dynamics is a well-established technique for studying melting in clusters and bulk. High-pressure melting has been simulated in systems as complex as MgSiO₃ and SiO₂ with periodic boundary conditions.¹¹ Clusters as small as 64 atoms of KCl have shown behavior similar to bulk melting,¹² and the primary differences between melting in clusters and bulk are shifts

in the melting temperature and surface melting.^{13,14} How cluster behavior evolves into bulk behavior with increasing size has been examined using both molecular dynamics¹⁵ and statistical mechanics.¹⁶ Our goal is to understand bulk melting, but we have chosen to study a range of cluster sizes rather than a periodic bulk system since enforced periodicity greatly inhibits crystallization from the liquid, especially in defect-free systems with long-range forces. By using finite clusters rather than periodic boundary conditions, both melting and crystallization begin readily at the surfaces, so that we can directly reverse the melting curve. We obtain both the melting (on heating) and crystallization (on cooling) temperatures, by which the equilibrium melting temperature must be bounded. With periodic boundary conditions *equilibrium* melting and crystallization are impossible to simulate without introducing extended defects;¹⁷ although the melting curve can be determined by free-energy integrations,¹⁸ the dynamics of the melt and crystal nucleation processes cannot be directly observed. By systematically studying different-sized clusters ranging from 64 to 1000 atoms, we can extrapolate to obtain bulk properties.

Lindemann¹ proposed perhaps the earliest instability model for melting, and related melting to the crystal shaking itself apart at the melting point. He proposed that melting occurs when the rms displacements of atoms reach some fraction of the nearest-neighbor distance. The Lindemann law is often treated as an empirical approach for predicting melting,^{19,20} but fundamental tests have been few. Many applications and tests have been based on assuming a Debye model and used thermodynamic data for the Debye temperature Θ_D to obtain the melting temperature T_M with the expression $T_M = (Mk_B \Theta_D^2 a^2 / 9\hbar^2) \Delta^2$, where M is a reduced mass, a is the near-neighbor distance, and Δ is the rms displacement of the atoms relative to the near-neighbor distance

a at the melting point, which varies somewhat with different materials. For example, the experimental melting curve of Pb has been shown to agree well with Lindemann behavior based on a simple Debye-Grüneisen model fit to a pair potential obtained from first-principles electronic structure calculations up to 100 GPa.²¹ This is not a strong test of the Lindemann hypothesis, however, since it depends on harmonic Debye behavior, and on knowing *exactly* how the effective Θ_D varies with pressure and temperature. More sophisticated analyses²⁰ still require the harmonic and anharmonic response of the crystal along the melting curve, so that apparent failures of Lindemann's model may instead reflect failures in the lattice-dynamical description of the crystal, particularly near melting, or ambiguities in how to apply the Lindemann criterion to complex crystals. Such empirical thermodynamic tests of Lindemann's law have generally shown it to be unreliable for predicting melting curves even for simple alkali halides.²⁰ Notable fundamental studies include simulations for argon using a Lennard-Jones potential,²² Monte Carlo simulations used in conjunction with perturbation theory for general Lennard-Jones systems,²³ and a self-consistent phonon study of Lennard-Jonesium and the Gaussian core model.²⁴ All of the atomistic studies found that Lindemann's model predicted melting well, at least in the classical (i.e., high-temperature) regime. However, all of these rigorous tests have been based on simple monatomic systems with idealized potentials. In particular, it can be shown that a power-law potential such as the repulsive part of a Lennard-Jones potential obeys Lindemann's law exactly, and since the attractive part can be treated as a small perturbation at high temperatures,²³ it is not surprising that Lindemann's law is followed closely for Lennard-Jonesium. Thus, in spite of the venerable age of Lindemann's criterion, no fundamental atomistic study using realistic potentials for a more complex system has been reported until now.

Another line of approach relating crystalline instabilities to melting began with Born in 1939,² who proposed that crystals transform to melts, gels, or gases when they become elastically unstable with respect to the shear elastic constants c_{44} , $c_{11}-c_{12}$, or to the bulk modulus K , respectively, as temperature or pressure varies. Boyer³ suggested that the vanishing of bulk moduli with increasing temperature that he found in Gordon-Kim models²⁵ of alkali halides was related to melting. Isaak, Cohen, and Mehl⁹ found for the same potential used here that the quasiharmonic free energy as a function of strain gives a vanishing $c_{11}-c_{12}$ *before* the occurrence of the instability in the bulk modulus, and also found the elastic instability to occur very close to the experimental zero-pressure melting point. There has been much hesitation to relate this instability directly to melting because melting is a first-order phase transition with a transition point given by the equality of the free energies of the phases (e.g., Ref. 26). However, the thermodynamic argument gives no information on the microscopic origin of melting, and more specifically does not rule out the importance of a lattice instability in driving a phase transition. For example, ferroelectric transitions in BaTiO₃ and PbTiO₃ are

first order, and the transition points are given by the equality of the free energies of the ferroelectric and paraelectric phases. Nevertheless, there is a well-defined soft-mode lattice instability associated with the transitions. Due to complications related to domain formation and long-range strain interactions the soft-mode frequency does not vanish at the phase transitions, and there is now much evidence that there is a crossover to order-disorder type behavior as the ferroelectric phase transition is approached.²⁷ So the first-order nature of a transition does not rule out an underlying dynamical instability in the phases. Molecular-dynamics (MD) simulations for Cu show just this behavior; $c_{11}-c_{12}$ would vanish at $T=1430$ K, but a first-order transition occurs earlier at 1170 K while $c_{11}-c_{12}$ is still finite.¹⁷

II. METHODS

A. Potential

It is important to use an accurate, well-tested potential or one can be easily misled. For example, inverse power-law potentials automatically obey Lindemann's law along the melting curve due to their scaling properties,²² and Lennard-Jones potentials may mimic that behavior since the attractive part can be considered as a small perturbation on the repulsive power-law potential.²³ We have chosen the potential-induced breathing model since it has been extremely well tested against both experiments and electronic structure and total-energy calculations; the PIB model appears to be ideal for MgO.⁹ The PIB model is a Gordon-Kim-type²⁵ model, in which the charge density is approximated as spherical, overlapping, closed-shell ions. It differs from rigid-ion models in that the ions are allowed to relax spherically in response to changes in the long-range electrostatic potential. Since O²⁻ is unstable in the free state, the O²⁻ ion is stabilized by including a positive sphere in the atomic calculation, and the radius of the so-called Watson sphere is chosen to equal the long-range electrostatic potential at the ion. The total energy is calculated using the local-density approximation for the kinetic energy as well as for the electrostatic, exchange, and correlation energies. The total energy is given by a sum of three parts, the self-energy of each ion, the overlap energies between ions, and the long-range electrostatic or Madelung energy. Since the oxygen density depends on the long-range atomic environment, the pair interactions, as well as the self-energy, depend on the positions of all of the other ions. The PIB model gives much improved thermoelastic properties over rigid-ion models. PIB is a many-body model and not only gives the correct Cauchy violations, but gives the correct temperature dependence of $c_{12}-c_{44}$.⁹ Since the potential is long ranged and all N^2 interactions must be summed at each time step, well-converged computations were possible only by using a massively parallel architecture.²⁸ We used a modification of the massively parallel code developed for Lennard-Jonesium by Boyer and Edwardson for the CM-2.²⁹

One important question is whether the PIB potential is appropriate for clusters, particularly among the surface

atoms. Rigid-ion models for clusters show that with ionic charges Mg^{1+} and O^{1-} the bulk rocksalt structure is favored even for clusters as small as 20–50 atoms, but that clusters with ± 2 charged ions favor open rings.³⁰ There appears to be little question, however, that clusters of 1000 atoms are cubic and bulklike.^{30,31} The PIB potential has the advantage over rigid-ion potentials in that one primary difference between the surface and bulk atoms, the reduction in Madelung potentials, is reflected in the potential. It is possible that ionic charges also vary from the surface to the bulk, and this is not reflected in the present calculations. Our goal here, however, is to understand bulk melting, and, by studying cubic clusters as a function of cluster size, we can recover good estimates of bulk properties.

B. High-pressure molecular-dynamics simulations

We performed classical MD simulations using the Verlet algorithm with time steps ranging from 0.25 to 3 fs. The zero-pressure simulations were performed for a clus-

ter in free space, and pressure was simulated by enclosing the cluster of atoms in a cubic box with a size chosen to give the average pressure of interest. All simulations were at constant energy and number, and the high-pressure runs were at constant volume. The pressure was calculated both by the virial and by momentum transfer to the box walls and both numbers agreed to 0.5%. At high pressures, desired average pressures were obtained by scaling the velocities (that is, by varying the temperature) but velocity scaling was not used after equilibration for the portions of the runs used for evaluating correlation functions or melting. All N^2 interactions were calculated without truncation. The PIB potential is a many-body potential, and the pairwise interactions depend on the Madelung potential at each atom in a pair; the Madelung potential at each atom was calculated from the other $N-1$ atoms at each time step. For the 1000 atom clusters, simulation times ranged from 5 to 640 ps, and runs up to 430 000 time steps were used to obtain highly accurate rms displacements and well-constrained melting and crystallization points.

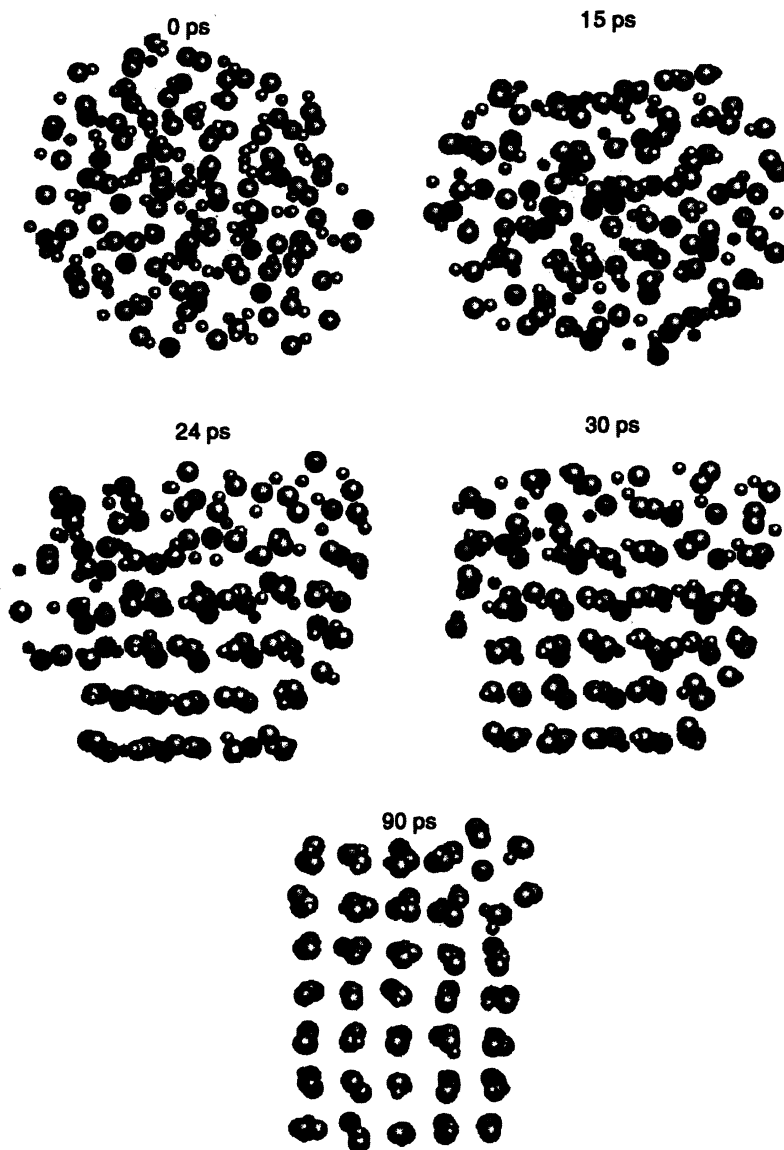


FIG. 1. Five frames are shown from an animation, showing nucleation and crystallization of a cluster of 216 atoms of MgO at zero pressure in free space. The droplet in this figure was heated until it melted and then supercooled to about 1000 K below the melting point. Newton's equations were then integrated at constant energy. The nucleation and growth process is quite fascinating. First flat faces form on the cluster (see 15 ps). These flat faces appear and disappear until one stabilizes by inducing layering in the oxygen ions throughout the cluster. After this rough organization of the cluster, the crystal nucleation is completed by ordering of the magnesium ions on the nucleation surface. Then crystal growth begins in earnest and both crystalline and molten regions coexist with a well defined interface (24–30 ps). The crystal that nucleated was only five atoms across due to the radius of curvature of the droplet, rather than the six across that could make a perfect cube. Thus a defect results, in this case a textbook example of a low-energy defect, a rounded corner. During the crystallization process, atoms diffuse very rapidly on the surface. At higher pressures we found almost no hysteresis.

III. RESULTS

A. Melting curve

Simulations were studied by computer animations, and melting and crystallization clearly initiated at the cluster surfaces. Figure 1 shows a sequence of crystallization from the melt. The crystal nucleates on one surface and then grows, during which time both crystalline and melt regions coexist in spite of the small cluster size. No evidence for surface precursor melting was observed in the animations. This is most likely due to the stability of the (100) faces of MgO, similar to the (100) and (111) faces of Cu for which no surface premelting has been seen.³²

Figure 2(a) shows a set of hysteresis or van der Waals loops in temperature versus energy that were obtained by heating and cooling. On heating, the temperature decreases as the cluster melts, and on cooling, the temperature increases during crystallization, due to the enthalpy of melting. Figure 2(b) shows the resulting melting curves, and the black band in the inset indicates the hysteresis between melting on heating and crystallization on cooling. The melting curves show strong curvature at low pressures due to the greater compressibility of the liquid than the solid, and there is a pronounced size effect, which increases with increasing pressure. Figure 2(c) shows the melting temperature versus the inverse cluster length; surprisingly, this relationship is quite linear even for cluster sizes as small as 216 atoms, and departs only slightly from linearity for clusters as small as 64 atoms. This gives us confidence to extrapolate to infinite cluster size and to give the bulk melting temperatures in Fig. 2(b). Note that the zero-pressure melting point is predicted to be 3200 ± 500 K for the PIB potential, which agrees well with the experimental value of 3098 K. The bracket for the melting temperature at zero pressure is large due to hysteresis for melting versus crystallization for the free cluster, which is large at zero pressure (590 K for the 1000-atom cluster and 330 K for the 216-atom cluster), but becomes negligibly small with in-

creasing pressure. Nevertheless, hysteresis is much worse with periodic boundary conditions. There are no experiments for effects of pressure on melting in MgO, so our high-pressure melting curve is a prediction, which will be compared with future experiments.

We also performed lattice dynamics using the same potential. Figure 2(b) also shows the quasi-harmonic instability $c_{11}-c_{12} \rightarrow 0$. Although the elastic instability corresponds closely to the experimental and MD melting points at zero pressure, it deviates from them with increasing pressure [Fig. 2(b)].

B. Root-mean-squared displacements along the melting curve

The simple elastic instability model does not follow the pressure dependence of melting, although it does correspond to melting at zero pressure. In Fig. 2(b) we show the thermodynamic Lindemann criterion for melting computed using the quasi-harmonic free energy for the same PIB potential, with the zero-pressure melting point anchored to the experimental melting point. We used the relationship²⁰ $-d \ln T_m / d \ln V_m = 2\gamma - 2/3$ and fixed the zero-pressure melting point to be equal to the experimental value. This is similar to previous empirical applications of the Lindemann law, except that we have calculated the quasi-harmonic rms displacements with lattice dynamics using the same potential as was used for the MD simulations. Although there is some correspondence between the thermodynamic Lindemann melting curve and the predicted MD bulk melting ($N \rightarrow \infty$), the agreement is not sufficient to base any strong conclusions on the accuracy of the physics behind the Lindemann model.

A clear and most surprising picture emerges when the actual anharmonic rms displacements are computed from the MD results, rather than from quasi-harmonic lattice dynamics. These were obtained from the intercept (small time limit) of the mean squared displacement versus time,

$$\langle [r(t) - r(0)]^2 \rangle = (2u_{\text{rms}})^2 + 6Dt,$$

where D is the diffusion constant and the ensemble aver-

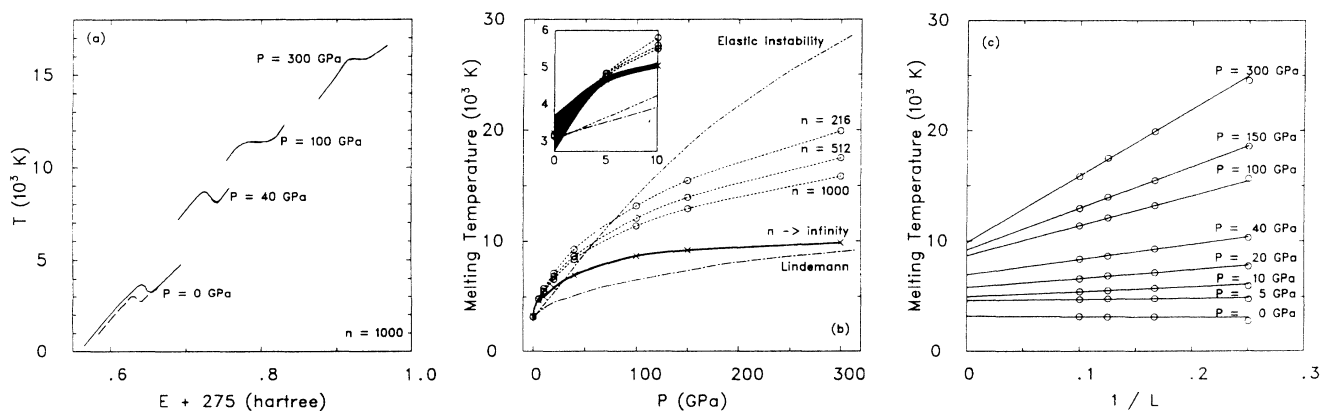


FIG. 2. (a) Melting loops on heating (solid) and cooling (dashed) 1000-atom clusters. Only at zero pressure do we find significant hysteresis. The melting temperature is at the center of each melting loop. (b) Melting curves for 216-, 512-, and 1000-atom clusters and the extrapolated melting curve for bulk MgO. The inset shows the low-pressure region, and the thick band in the inset indicates the hysteresis. Also shown is the $c_{11}-c_{12} \rightarrow 0$ elastic instability, and the thermodynamic Lindemann criterion obtained using quasi-harmonic lattice dynamics. (c) The size dependence of the melting temperature. $L = N^{1/3}$ is the length of the cluster. The solid lines were fit to the 216-atom and larger clusters, but come close to the 64-atom clusters, which were not used in the fit. The bulk melting temperatures shown in (b) are extrapolated from the intercepts for $1/L \rightarrow 0$.

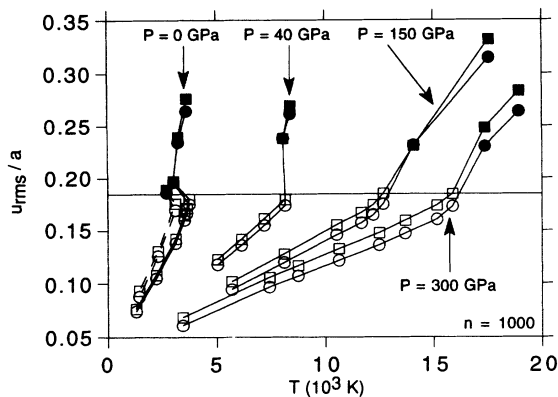


FIG. 3. Lindemann ratio u_{rms}/a versus temperature for 1000-atom clusters as a function of pressure. Circles are for O and squares are for Mg. The open symbols are for crystal and the filled symbols are for liquid, runs within the hysteresis loops were not included since they show both solid and liquid regions. Melting occurs when the rms displacements reach about 18% of the near-neighbor distances over the entire pressure range.

age is over all initial times and atoms. The factor of 2 arises since $r(0)$ does not refer to a fixed lattice but rather to each instantaneous configuration. Figure 3 shows the rms displacements over the near-neighbor distances of the O and Mg ions ($u_{rms}/\langle a \rangle$) as functions of temperature and pressure calculated accurately from the MD simulations. At the melting point the change in u_{rms} be-

comes large or is discontinuous, and there is good agreement with the melting temperatures shown in Fig. 2(a). The major result is that melting occurs at constant rms displacement relative to the average near-neighbor distance from zero pressure to 300 GPa. We find this behavior invariant with respect to cluster size for the clusters from 64 to 1000 atoms; although the melting temperature changes with cluster size, melting always occurs at a constant $u_{rms}/\langle a \rangle = 18\%$. This number is not significant in itself, although it is somewhat larger than is observed for other compositions. What is significant is that it is constant as a function of pressure.

C. Liquid structure along the melting curve

We have studied the liquid and solid structures and have calculated pair distribution functions, coordination numbers, and three-body angular distributions, along the melting curve. Figure 4 shows the calculated pair distribution functions for crystal and liquid. Since we are comparing structures along the melting curve, the high-pressure distribution is also at much higher temperature. Due to the high temperatures, the crystalline peaks are quite broad, and of similar but slightly sharper breadth than the liquid peaks. At large distance $g(r) \rightarrow 0$ rather than 1 due to the finite cluster size. The crystalline order extends to the edge of the cluster, but in the liquid, order at both zero and high pressures decreases more rapidly. However, medium-range order in the liquid persists over

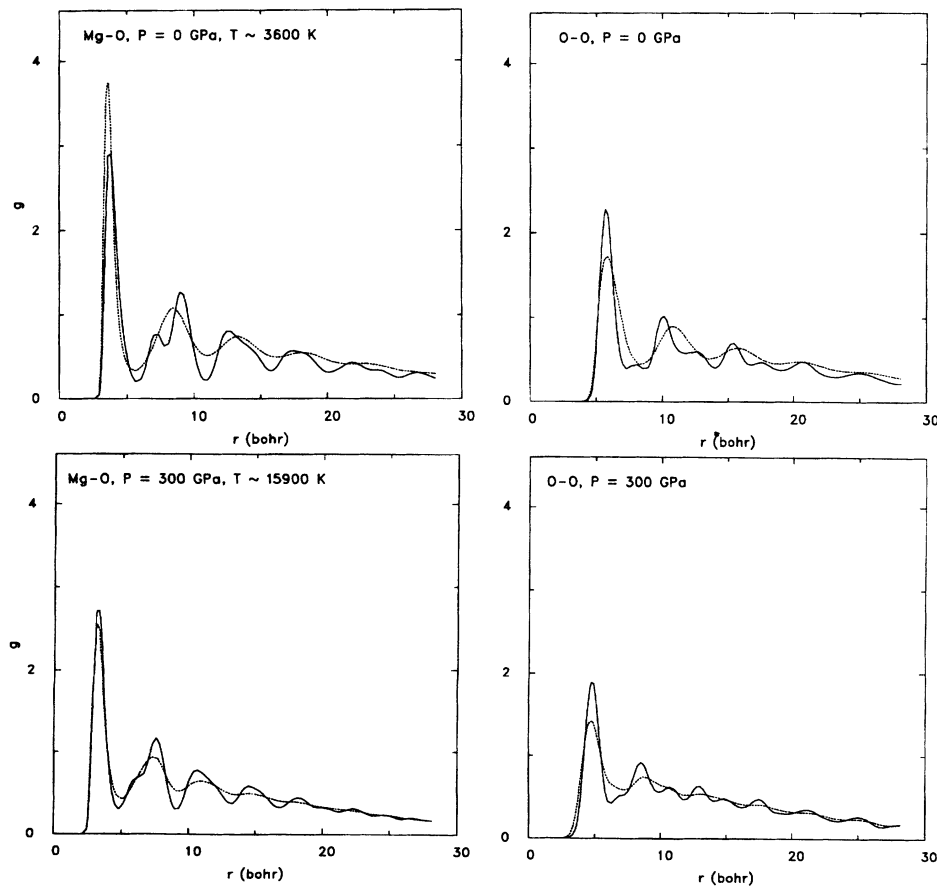


FIG. 4. Partial pair distribution functions at $P=0$ and $P=300$ GPa for crystal (solid) and liquid (dashed) near melting. The distribution functions vanish with increasing r rather than tending to unity due to the finite cluster size.

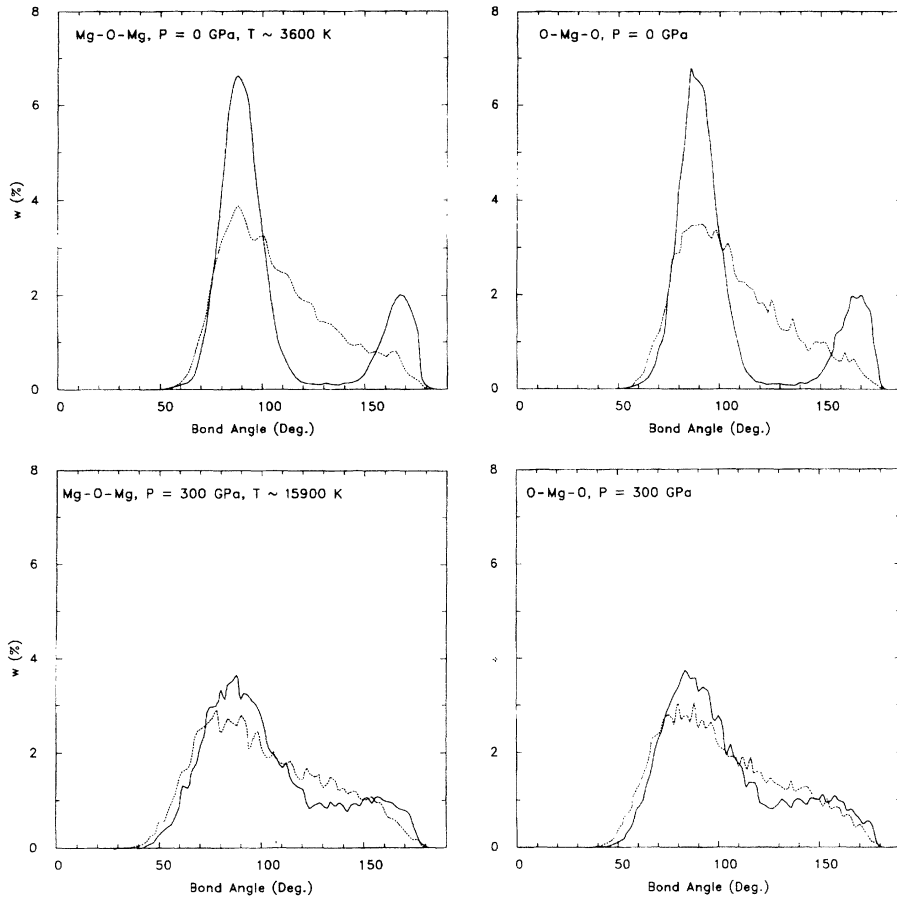


FIG. 5. Angular distribution functions at $P=0$ and $P=300$ GPa for crystal (solid) and liquid (dashed) near melting.

several shells of neighbors to over 15 bohr. At high pressures the first coordination shell in the liquid is almost identical to that in the solid. That is shown even more clearly in Fig. 5 where angular distributions averaged over the first peak in the Mg-O pair correlation function are shown. The crystalline distribution peaks at 90° as expected. The peak which is at 180° in the ideal crystal at 0 K is shifted to lower angles due to thermal motion. At zero pressure the crystalline and liquid angular distributions are quite different, but the liquid distribution is still peaked near 90° . At high pressures and temperatures the

liquid and solid angular distributions are very similar, indicating converging local structure with increasing pressure.

The convergence of local liquid and solid structure is most evident on examination of coordination numbers. Figure 6 shows the average coordination numbers for the liquid and solid as a function of pressure along the melting curve. Since the melting temperature increases with increasing pressure, temperature increases along the abscissa, leading to the slight apparent decrease in the crystal coordination number with increasing pressure.

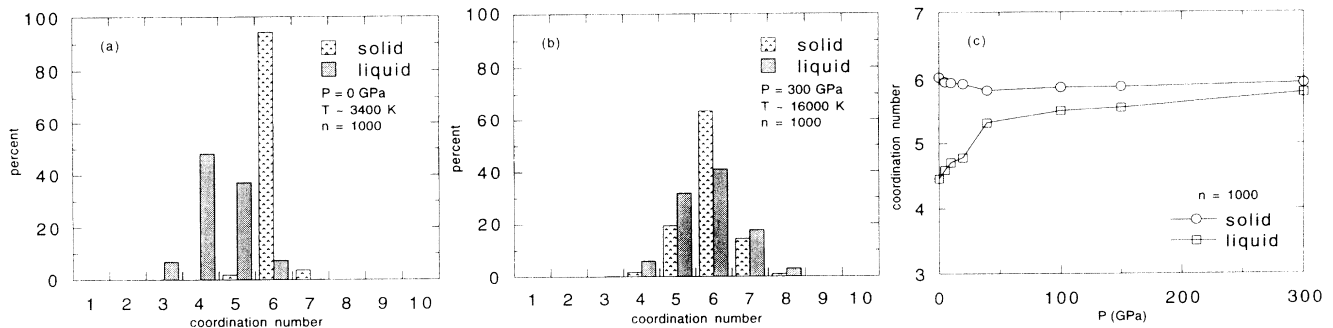


FIG. 6. Coordination numbers for solid and liquid MgO at (a) zero pressure, (b) 300 GPa, and (c) along the melting curve. The liquid coordination number increases continuously from 4.5 to 6 as pressure is increased, and the liquid and crystal become more similar in structure.

Whereas the average coordination number in the crystal is approximately 6 as expected, the melt has a coordination number of 4.5 at zero pressure, which increases gradually with increasing pressure. Similar behavior is seen in alkali halides at zero pressure.³³ Though the coordination number is close to 4 in the liquid, it is not due to regular tetrahedrally coordinated ions because we find the bond angles to peak near 90° as expected for octahedral coordination (Fig. 5).

D. Equation of state along the melting curve

We have also fitted the volumes of the crystal and liquid along the melting curve to a Birch equation of state³⁴ giving $V_0=21.0 \text{ \AA}^3$, $K_0=149 \text{ GPa}$, and $K'_0=3.47$ for the solid and $V_0=27.0 \text{ \AA}^3$, $K_0=59.2 \text{ GPa}$, and $K'_0=3.83$ for the liquid (rms errors from these fits are 3 GPa). Note that these are nonisothermal equations of state. The results are shown in Fig. 7. In spite of the much greater compressibility of the liquid than the solid at low pressures, the densities of the solid and liquid do not cross, even on extrapolation above the highest simulation pressure of 300 GPa, due to the higher K'_0 for the liquid. The convergence of liquid and solid densities along the melting curve is discussed further below.

E. Thermodynamics of melting at high pressures

We have determined the basic thermodynamic parameters for melting from our simulations (Fig. 8). The enthalpy change on melting, ΔH_m , was obtained from the integrated energy versus temperature over the melting interval, and ΔS_m was obtained from the slope of the melting curve and the Clapeyron equation $dT/dP = \Delta V_m / \Delta S_m$. If we consider $T_m = \Delta H_m / \Delta S_m$, we see that the increase in ΔH_m with pressure is the primary cause of the increase in T_m with pressure. The entropy of

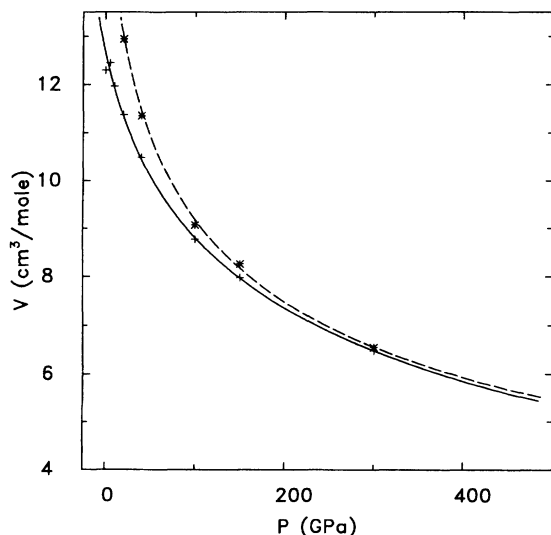


FIG. 7. Equations of state of crystal (solid) and liquid (dashed) along the melting curve.

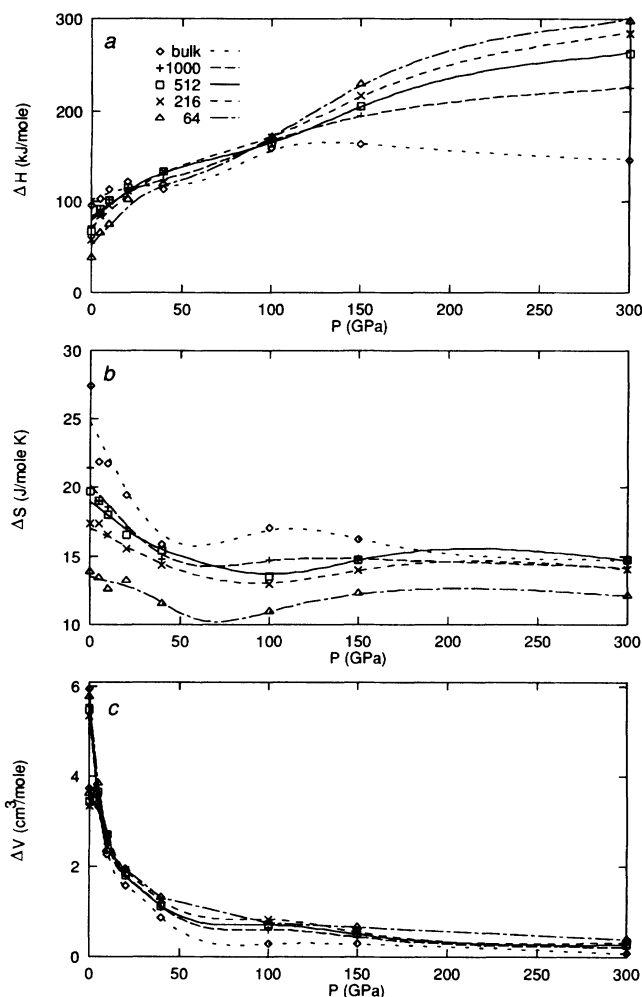


FIG. 8. Thermodynamic parameters for melting as a function of system size. The lines are only guides for the eye. The bulk curves were obtained by extrapolation of the 216-, 512-, and 1000-atom cluster results vs $1/L$. All results shown were obtained on heating. On cooling results were essentially identical except at zero pressure for 216-atom clusters and larger, in which case defects were frozen in on quenching. (a) ΔH_m determined from equal-area constructions on the E vs T results [Fig. 2(a)] plus $P\Delta V_m$. Note the change in sign of the size effect at about 40 GPa, perhaps due to increasing importance of the long-range Madelung terms at high pressures and greater importance of short-range coordination changes at low pressures. (b) ΔS_m determined from the Clapeyron relation $dT/dP = \Delta V / \Delta S$ using the slope of the melting curve and ΔV_m . At high pressure ΔS_m converges very rapidly with system size. (c) ΔV_m determined from the change in box size required to keep constant average pressures at high pressures. At zero pressure Boyer and Pawley's method (Ref. 28) was used to determine the average density of the cluster, which involves a Gaussian weighted average over each atom position and is therefore more surface sensitive. We also estimated ΔV_m from $dT/dP = T\Delta V / \Delta H$ and that is shown as the upper set of points at zero pressure. ΔV_m drops most rapidly at low pressures where the liquid structure changes rapidly with increasing pressure. At high pressures ΔV_m becomes small and seems to asymptotically approach zero.

melting also decreases with increasing pressure [Fig. 8(b)], decreasing most rapidly in the low-pressure regime where the liquid structure changes most rapidly with pressure [Fig. 6(c)]. Of particular interest is the high-pressure limiting behavior for melting. As discussed above, ΔV_m remains finite even on extrapolation of these equations of state to 500 GPa.

IV. DISCUSSION

A. Liquid versus solid structure at high pressures

A clear result of the present simulations is that local liquid and solid structures converge with increasing pressure, and the liquid approaches crystalline densities with increasing pressure. Long-range order is not present in the liquid, but its packing approaches crystalline efficiency. Examination of individual frames (snapshots) from computer animations shows very high degrees of order at high pressures throughout the cluster. In spite of the high degree of order at any instant, there are rapid cooperative diffusive motions of atoms as would be expected in a liquid. The diffusive motions seem to involve mainly two-body exchanges. The coordination number in the liquid increases with increasing pressure, and the greater compressibility of the liquid than the solid is due to this. Similar changes have been proposed for silicate liquids.^{35,36} If one considers silicate melts as essentially oxide melts, since the oxygen ions make up by far the majority of the volume of the melt, the results here for MgO may be extended to make general predictions for the structural and melting behavior of silicate melts at high pressures. Once the liquid coordination number becomes similar to that of the solid (50–100 GPa for MgO), the liquid and solid compressibilities become similar, so that the greater compressibility of liquids is essentially a relatively low-pressure phenomenon.

B. Lattice instabilities

At zero pressure the melting point and the quasiharmonic instability $(c_{11}-c_{12})_{\text{QH}} \rightarrow 0$ seem to coincide in MgO. Similar behavior is observed for alkali halides.³ This behavior thus spans a wide range of compositions and melting points, and thus it seems far fetched to assume that such behavior is entirely fortuitous. However, at high pressure this relationship breaks down, as is shown in Fig. 2(b). The relationship of the quasiharmonic instability with melting is unclear, because the actual, anharmonic elastic constants show an instability at higher temperatures, above the actual melting point.¹⁷ One possible interpretation is that the quasiharmonic instability is correlated to barrier heights to bulk diffusive motion, and that melting occurs when the kinetic energy of sufficient numbers of atoms is greater than the barrier height to drive a structural instability and thus a phase transition. If this picture is correct, it is unclear why the quasiharmonic instability fails to correspond to melting at high pressures. The failure of $(c_{11}-c_{12})_{\text{QH}} \rightarrow 0$ to correspond to melting at high pressures is probably not due to the approach of a coordination change (which is predict-

ed to occur at much higher pressures, ~ 500 GPa in the solid)^{9,10} or to increasing defects in the crystal or melt with increasing pressure and temperature, because we see no such evidence in our simulations. Perhaps the simple elastic instability is fortuitously close to important barrier heights at zero pressure. For example, Boyer and co-workers³⁷ have proposed that the magic strain coordinates, the strains that transform a *B1* lattice into an equivalent *B1* lattice but with a different orientation, are the lowest-energy coordinates for lattice strain. However, we see no evidence for such cooperative all-body motions in our simulations, yet our clusters melt at close to the experimental melting point at zero pressure. Rather we see evidence for exchange processes in the melt that lead to high mobility.

We find using quasiharmonic lattice dynamics that Lindemann's law does not agree very well with the melting curve obtained in our simulations. On the other hand, we find that the Lindemann criterion is strongly obeyed when the actual, anharmonic, rms displacements are calculated from the MD simulations, rather than assuming quasiharmonic behavior up to melting. If our potential was close to an inverse power-law potential, this would tell us nothing about the dynamics of melting, because power-law potentials automatically scale along the melting curve and liquid and melt structures remain constant along the melting curve. The fact that we find changes in liquid structure along the melting curve is proof that the behavior we find is not due to scaling laws for the potential. In fact, the PIB potential is very far from a power-law potential in any case, since it includes large many-body terms in the self-energy, Madelung contributions, and a short-range potential with both attractive and repulsive parts. The PIB potential is expected to be very realistic for the behavior of MgO based on comparisons with both self-consistent electronic structure calculations¹⁰ and experiment.⁹

We emphasize again that the Lindemann relationship we have discovered in our simulations of MgO is not due to the potential being in any way like a power law. Inverse power-law potentials give $\Delta V_m/V_c$ and ΔS_m to be constant³⁸ which is clearly not so for our potential (Figs. 8 and 9). If the observed Lindemann behavior is not due to dimensional scaling, what could be its cause? The behavior indicates that the approach to melting can be inferred by examining only properties of the crystal. This is true in spite of changes in liquid structure along the melting curve. This seems to require an underlying dynamical instability in the solid as the melting transition is approached.

C. One-phase vs two-phase melting models

The fact that melting is predictable from behavior of the solid alone, despite changes in liquid structure along the melting curve, is strong support for instability or one-phase models for melting. One-phase models suggest that melting can be predicted from the behavior of one phase alone, without regard to the other. They do not necessarily imply that two phases do not coexist at the transition, or that the transition is not strongly first or-

der. Arguments that melting can only be understood in terms of free-energy differences between solid and liquid (i.e., two-phase theories) ignore the success of soft-mode and order-disorder phase transitions in solids, which are also often first-order phase transitions. However, two-phase models cannot explain the apparently intrinsic instabilities in solid and liquid phases on approach to melting.

Even though melting is incontrovertibly a first-order thermodynamic phase transition, our results suggest that it is related in a fundamental way with intrinsic instabilities in the solid. Finding these intrinsic instabilities will lead to a fundamental microscopic picture of melting. A search for low-frequency structure in $S(q, \omega)$ in the crystal near melting may be fruitful. On the other hand, the intrinsic instability cannot be the whole story; if one were to introduce another component into the liquid that is not soluble in the solid, for instance, the melting temperature would decrease due to the increased entropy of the liquid phase. One-phase models are not in contradiction to thermodynamics, but they simply propose that an instability in one phase leads to a rapid increase in the free energy of that phase relative to another, thus driving a phase transition.

D. Melting at extreme pressures; predictions

As $\Delta V_m/V_c \rightarrow 0$ with increasing pressure, and as the packing of the liquid becomes by necessity as efficient as that of the solid, what is the nature of the melting transition? Most clearly we find that melting is not simply due to changes in packing density. The changes in packing density increase with increasing pressure, and the density difference between solid and liquid slowly vanishes, yet the entropy and enthalpy changes, ΔS_m and ΔH_m , remain large, indicating that packing density is not a good primary order parameter. On the other hand, rapid diffusive motion sets in immediately on melting at all pressures. This implies that the dynamical changes on melting are the most important, and at high enough pressures the dynamical changes at the transition dominate.

Most intriguing, we find that ΔS_m is still large in this limit. Figure 9 shows ΔS_m vs $\Delta V_m/V_c$; the relationship is linear within the precision of the results, although saturation to a constant entropy of melting at extreme pressures cannot be ruled out. A linear relationship is intriguing because ΔS_m vs $\Delta V_m/V_c$ is linear among simple substances at zero pressure with an intercept of $\Delta S_m/(k_B \text{ atom}) = 0.7$, which has been related to the ratio of the free volume of the liquid to that of the solid.³⁸ Since in the extreme high-pressure limit the packing of the liquid must approach that of the solid, the free volumes must also approach, and we indeed find for our bulk extrapolation $\Delta S_m/(k_B \text{ atom}) = 0.95 \pm 0.1$, which is consistent with the free volumes being equal. The entropy of melting becomes almost entirely communal,³⁹ or dynamic⁴⁰ and diffusive, in the high-pressure limit. In other words the entropy change can be envisioned as a change in available phase space for each atom; in the crystal each atom is more or less confined to a single cell, whereas in the liquid diffusive motion allows each atom to move

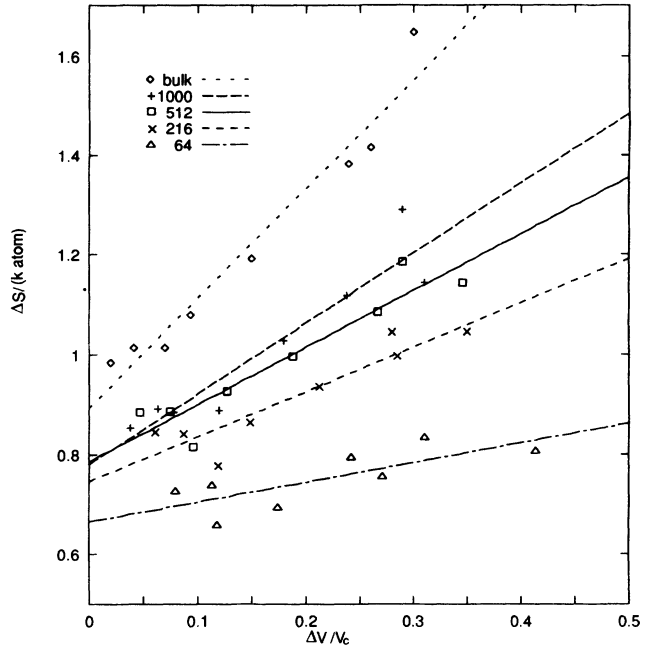


FIG. 9. $\Delta S_m/(k_B \text{ atom})$ vs $\Delta V_m/V_c$. The relationship is linear within the precision of the data. The scatter is due to multiple interpolations needed to obtain these numbers for the finite number of simulations. The implication of $\Delta S_m/(k_B \text{ atom}) \rightarrow 1$ as $\Delta V_m/V_c \rightarrow 0$ is that the entropy of melting becomes purely collective or diffusive in the high-pressure limit.

throughout the volume. The full communal entropy at high pressures is contrary to expectations that the communal entropy would vanish at high densities.⁴¹ In the high-pressure limit, our results show that the atomic motions in the liquid must be such as to allow for preservation of local coordination and structure as in the solid. Animations show that large-scale motions at high pressure are dominated by exchange and many-body motions. The entropy change at lower pressures contains both this communal contribution and the static contribution from structural disorder in the liquid.

There are presently no experimental data on melting of MgO at high pressures. Quantities that have been predicted here include the melting curve, rms displacements which are related to diffraction linewidths, equations of state, and ΔH_m , ΔS_m , and V_m . The greatest uncertainty in the present study is in the extrapolation from small clusters to the bulk, and this extrapolation becomes larger with increasing pressure. The zero-pressure density of the liquid is also rather poorly determined; due to the free boundary conditions the volume is not well defined. The qualitative behavior of the thermodynamic functions, the validity of the anharmonic Lindemann criterion, and the structural changes with pressure should be robust and most probably general for simple systems with solid and liquid structures which involve the same bonding character and share similar, simple local structure.

V. CONCLUSIONS

How general might be these results? MgO is in many ways a simple material, yet we propose that the phenomena observed here may be general. Although the crystalline structure of MgO is simple rocksalt, the liquid structure is more complex and does change with pressure, yet the Lindemann relation remains valid. The interatomic interactions in MgO are long ranged, but the Lindemann relation also seems to be obeyed in metallic Pb, which is dominated by short-range interactions. Do the relationships observed here exist in complex materials such as SiO₂? There appears to be no fundamental objection to the existence of intrinsic instabilities in all materials before melting; future work will clarify how general are the present results. If instabilities are intrinsic to melting, then any complete theory of melting must include such instabilities. In applications in geophysics and materials, a better understanding of the instabilities that drive melting will lead to better predictions of melting in new systems or outside the range of routine experimentation. X-ray studies of Debye-Waller factors near melting as a function of pressure would be particularly exciting.

The most important result of the present study is the implication that the dynamical aspect of melting, that is, the onset of large-scale diffusive motion, is more universal than packing and structural changes which are more ob-

vious at low pressures. At high pressures the entropy and enthalpy changes are large at melting, but the volume change becomes vanishingly small with increasing pressure, and local structure in the solid and liquid becomes identical.

In summary, we have performed large-scale simulations of high-pressure melting in MgO. We have predicted the melting curve, liquid and crystal structure, thermodynamic properties, and rms displacements as functions of pressure. We hope that these results will stimulate experimental and theoretical work on the fundamental instabilities that lead to melting.

ACKNOWLEDGMENTS

Computations were performed on the CM-5, CM-2, and Convex C-3 at NCSA, the CM-200 at NRL, and on IBM RS6000's at the Geophysical Laboratory. We acknowledge L. L. Boyer for helpful discussions and for allowing us to use his CM-2 MD code which we modified for the present study. We thank D. G. Isaak for performing the lattice-dynamics computations of c_{11} - c_{12} and the thermodynamic Lindemann results, and C. Bates for assistance with the computer animations. We thank R. J. Hemley, C. Meade, and J. Feldman for helpful discussions and comments on the manuscript. This research was supported by the National Science Foundation EAR-9117932 and by the Office of Naval Research.

¹F. A. Lindemann, *Phys. Z.* **11**, 609 (1910).

²M. Born, *J. Chem. Phys.* **7**, 591 (1939).

³L. L. Boyer, *Phase Transitions* **5**, 1 (1985).

⁴J. L. Tallon, *Nature* **342**, 658 (1989).

⁵J. L. Tallon, W. H. Robinson, and S. I. Smedley, *Nature* **266**, 337 (1977).

⁶L. Verlet, *Phys. Rev.* **165**, 201 (1968).

⁷R. M. J. Cotterill, *J. Cryst. Growth* **48**, 582 (1980).

⁸L. L. Boyer *et al.*, *Phys. Rev. Lett.* **54**, 1940 (1985); **57**, 2331 (1986).

⁹D. G. Isaak, R. E. Cohen, and M. J. Mehl, *J. Geophys. Res.* **95**, 7055 (1990).

¹⁰M. J. Mehl, R. E. Cohen, and H. Krakauer, *J. Geophys. Res.* **93**, 8009 (1988); **94**, 1977 (1989).

¹¹J. D. Kubicki and A. C. Lasaga, *Phys. Chem. Mineral.* **17**, 661 (1991); M. Matsui and G. D. Price, *Nature* **351**, 735 (1991); E. A. Wasserman, D. A. Yuen, and J. R. Rustad, *Earth Planet. Sci. Lett.* **114**, 373 (1993); *Phys. Earth Planet. Interiors* **77**, 189 (1993).

¹²J. P. Rose and R. S. Berry, *J. Chem. Phys.* **98**, 3246 (1993); **98**, 3262 (1993).

¹³P. Stolze, J. K. Norskov, and U. Landman, *Phys. Rev. Lett.* **61**, 440 (1988).

¹⁴F. Ercolessi, W. Andreoni, and E. Tosatti, *Phys. Rev. Lett.* **66**, 911 (1991).

¹⁵H.-P. Cheng and R. S. Berry, *Phys. Rev. A* **45**, 7969 (1992).

¹⁶H.-P. Cheng, X. Li, R. L. Whetten, and R. S. Berry, *Phys. Rev. A* **46**, 791 (1992).

¹⁷D. Wolf, P. R. Okamoto, S. Yip, J. F. Lutsko, and M. Kluge, *J. Mater. Res.* **5**, 286 (1990).

¹⁸J. Mei and J. W. Davenport, *Phys. Rev. B* **46**, 21 (1992).

¹⁹J. P. Poirier, *Phys. Earth Planet. Interiors* **54**, 364 (1989); D.

Berberi, L. Grigoryan, S. Rabinovich, E. Shash, and A. Voronel, *J. Phys. Condens. Matter* **4**, 10 139 (1992).

²⁰G. H. Wolf and R. Jeanloz, *J. Geophys. Res.* **89**, 7821 (1984).

²¹B. K. Godwal, C. Meade, R. Jeanloz, A. Garcia, A. Y. Liu, and M. L. Cohen, *Science* **248**, 462 (1990).

²²M. Ross, *Phys. Rev.* **184**, 233 (1969).

²³J.-P. Hansen, *Phys. Rev. A* **2**, 221 (1970).

²⁴L. K. Moleko and H. R. Glyde, *Phys. Rev. B* **30**, 4215 (1984).

²⁵R. G. Gordon and Y. S. Kim, *J. Chem. Phys.* **56**, 3122 (1972).

²⁶M. Ross and G. Wolf, *Phys. Rev. Lett.* **57**, 214 (1986).

²⁷K. A. Müller, Y. Luspain, J. L. Servoin, and F. Gervais, *J. Phys. (Paris) Lett.* **43**, L537 (1982).

²⁸L. L. Boyer and G. S. Pawley, *J. Comput. Phys.* **78**, 405 (1988).

²⁹L. L. Boyer and P. J. Edwardson, in *Proceedings of the 2nd Symposium on the Frontiers of Massively Parallel Computation, Fairfax, VA, 1988*, edited by R. Mills (IEEE, New York, 1988), p. 275.

³⁰P. J. Ziemann and A. W. Catleman, Jr., *J. Chem. Phys.* **94**, 718 (1991).

³¹J. M. Recio, R. Pandey, A. Ayuela, and A. B. Kunz, *J. Chem. Phys.* **98**, 4783 (1993).

³²H. Hakkinen and M. Manninen, *Phys. Rev. B* **46**, 1725 (1992); H. Hakkinen and U. Landman, *Phys. Rev. Lett.* **71**, 1023 (1993).

³³M. Amini, D. Fincham, and R. W. Hockney, *J. Phys. C* **12**, 4707 (1979).

³⁴F. Birch, *J. Geophys. Res.* **93**, 8009 (1988).

³⁵E. M. Stolper and T. J. Ahrens, *Geophys. Res. Lett.* **14**, 1231 (1987).

³⁶X. Xue, J. F. Stebbins, M. Kanzaki, P. F. McMillan, and B. Pie, *Am. Mineral.* **76**, 8 (1991).

³⁷M. J. Mehl and L. L. Boyer, *Phys. Rev. B* **43**, 9498 (1991); L.

L. Boyer, E. Kaxiras, and M. J. Mehl, in *Kinetics of Phase Transformations*, edited by M. O. Thompson, M. J. Aziz, and G. B. Stephenson, MRS Symposia Proceedings No. 205 (Materials Research Society, Pittsburgh, 1991), p. 447.

³⁸S. M. Stishov, *Sov. Phys. Usp.* **31**, 52 (1988).

³⁹J. Hirschfelder, D. Stevenson, and H. Eyring, *J. Chem. Phys.*

5, 896 (1937).

⁴⁰We use “dynamic” in the same sense that the vibrational entropy is dynamic, not to imply that momentum cannot be integrated out of the partition function.

⁴¹J. G. Kirkwood, *J. Chem. Phys.* **18**, 380 (1950).

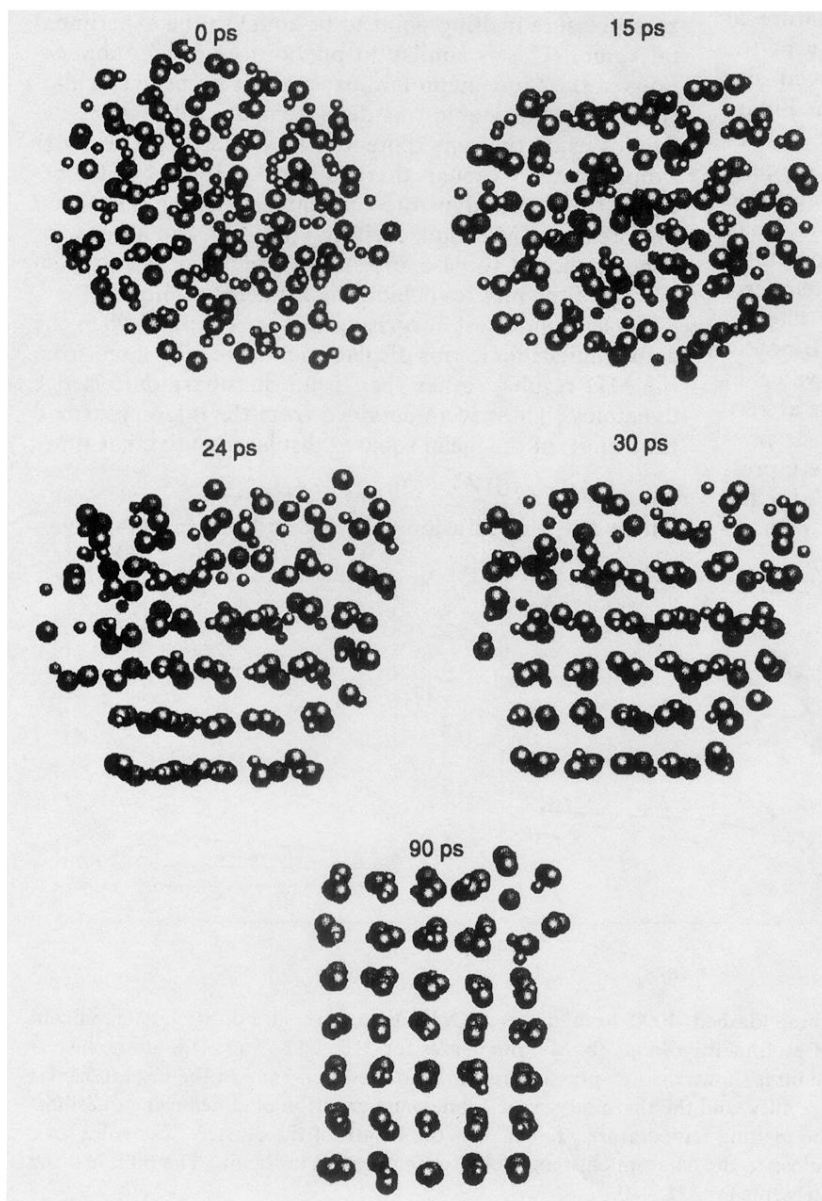


FIG. 1. Five frames are shown from an animation, showing nucleation and crystallization of a cluster of 216 atoms of MgO at zero pressure in free space. The droplet in this figure was heated until it melted and then supercooled to about 1000 K below the melting point. Newton's equations were then integrated at constant energy. The nucleation and growth process is quite fascinating. First flat faces form on the cluster (see 15 ps). These flat faces appear and disappear until one stabilizes by inducing layering in the oxygen ions throughout the cluster. After this rough organization of the cluster, the crystal nucleation is completed by ordering of the magnesium ions on the nucleation surface. Then crystal growth begins in earnest and both crystalline and molten regions coexist with a well defined interface (24–30 ps). The crystal that nucleated was only five atoms across due to the radius of curvature of the droplet, rather than the six across that could make a perfect cube. Thus a defect results, in this case a textbook example of a low-energy defect, a rounded corner. During the crystallization process, atoms diffuse very rapidly on the surface. At higher pressures we found almost no hysteresis.

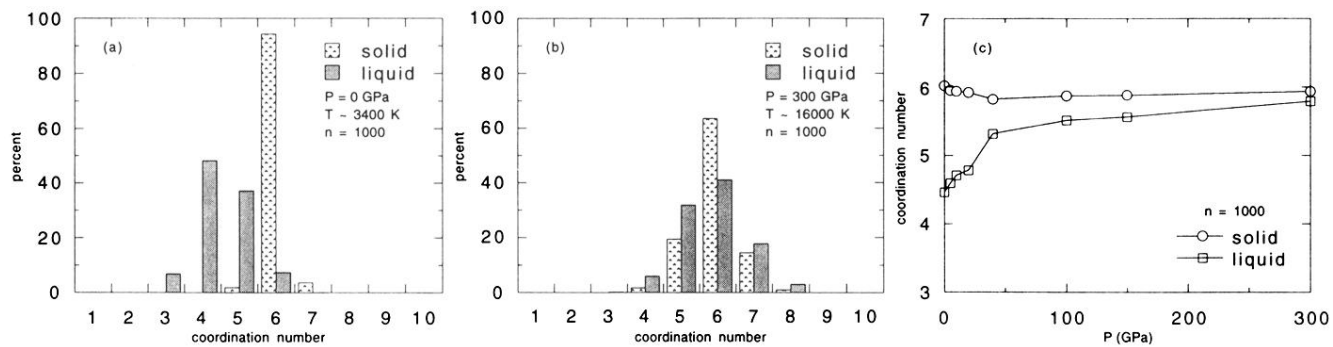


FIG. 6. Coordination numbers for solid and liquid MgO at (a) zero pressure, (b) 300 GPa, and (c) along the melting curve. The liquid coordination number increases continuously from 4.5 to 6 as pressure is increased, and the liquid and crystal become more similar in structure.